http://dx.doi.org/10.1109/LRA.2021.3098915

Intelligent Locomotion Planning with Enhanced Postural Stability for Lower-Limb Exoskeletons

Javad K. Mehr[1,2*], Mojtaba Sharifi[1,2], *Member, IEEE*, Vivian K. Mushahwar[2], *Member, IEEE*, Mahdi Tavakoli[1], *Senior Member, IEEE*

***Abstract*—In this paper, an integrated control strategy is developed for both locomotion trajectory planning and postural stability, enabling shared autonomy between the human and lower-limb exoskeleton. Divergent component of motion (DCM) analysis was employed previously based on the linear inverted pendulum flywheel (LIPF) model to regulate the position of the center of mass (CoM) for humanoid robots. In this study, a new extended model is investigated for the DCM analysis by replacing the previous LIPF model, which is tailored for multi-degree-of-freedom (DOF) exoskeletons. This new model is designed to be personalized for each specific user's body by relaxing the assumption of having the total CoM at the hip joint in the previous LIPF model. Accordingly, the exoskeleton has the authority to ensure the postural stability and viability of locomotion in this human-robot interaction (HRI) by adjusting the upper body position using a DCM-based hip correction strategy. Integrating adaptive central pattern generators (CPGs), the human has enough authority to modify the gait trajectories in real-time, while the amplitude and frequency of walking are constrained to their feasible ranges. The effectiveness of this intelligent controller for safe and stable locomotion is investigated through experimental studies on a lower-limb exoskeleton.**

***Index Terms*—Central Pattern generator (CPG), Divergent Component of Motion (DCM), Human-Robot interaction, Lower-limb exoskeleton, Adaptive motion planning.**

I. INTRODUCTION

SPINAL cord injuries, stroke, and multiple sclerosis are some causes of neurological impairments in the human gait. Millions of people affected by these conditions will be able to handle their daily activities and enhance their physical abilities by taking advantage of assistive and rehabilitative wearable systems (e.g., exoskeleton) developed in recent years [1]. The capabilities of exoskeletons in providing long-term repetitive movements, facilitating physical assistance and collecting users' motion data by their embedded sensory systems make them unique for lower-limb rehabilitation purposes [2]. Despite all of the advantages of employing exoskeletons in medical applications, providing adaptable trajectories and gait features that can be amended by the wearer while preserving the postural stability autonomously still needs to be addressed to provide compliant and safe human-robot interaction (HRI) [3].

Divergent component of motion (DCM) analysis was employed in trajectory generation for the center of mass (CoM) in bipedal locomotion of humanoid robots [4]–[6]. In this method, a linear inverted pendulum (LIP) model was used to represent the bipedal movement, and the divergent part of the LIP dynamics was introduced as the DCM [7]. Considering this model, two strategies have been used to overcome the disturbance applied during the bipedal locomotion including the adjustments of the step time and length that affected the frequency and amplitude of the gait, respectively [8]. However, these strategies are not suitable for the exoskeleton applications, since the gait parameters (e.g., amplitude and frequency of walking) are desired to be regulated based on the wearer's intention. Studies have designed optimal controllers to combine both of these adjustment strategies in order to realize a stable walking for bipedal robots. In Khadiv et al. [8], and Jeong et al. [9], a higher cost was allocated to the regulation of the foot landing position in the objective function to keep the preplanned footprint as much as possible. Jeong et al. [6] employed a linear inverted pendulum flywheel (LIPF) model to extend the DCM adjustment strategy and introduce a hip strategy (applying torque to the upper body) for that purpose. Similar to the previous studies, an optimization approach was suggested to minimize the error between desired and actual DCM by regulation of the ankle and hip trajectories in addition to the step size and walking speed [6].

Englsberger et al. [10] presented an enhanced centroidal moment pivot (eCMP) and virtual repelling points to extend the DCM trajectory in 3D space. The DCM dynamics was utilized to determine required force for a stable bipedal walking over an uneven ground and to generate a smooth path for the eCMP point [10]. In a similar approach for 3D DCM planning [11], the foot landing position was controlled and the required ground reaction force (GRF) was determined based on a viscoelastic model for the foot contact. It is worth mentioning that DCM adjustment has not been utilized for the postural stability of users wearing lower-limb exoskeletons so far.

Manuscript received: February, 25, 2021; Revised May, 20, 2021; Accepted June, 30, 2021.

This paper was recommended for publication by Editor Jee-Hwan Ryu upon evaluation of the Associate Editor and Reviewers' comments. This research was supported by the Canada Foundation for Innovation (CFI), the Natural Sciences and Engineering Research Council (NSERC) of Canada, the Canadian Institutes of Health Research (CIHR), and the Alberta Jobs, Economy and Innovation Ministry's Major Initiatives Fund to the Center for Autonomous Systems in Strengthening Future Communities. (Javad K. Mehr is the corresponding author).

[1]Javad K. Mehr, Mojtaba Sharifi and Mahdi Tavakoli are with the Department of Electrical and Computer Engineering, and Sensory Motor Adaptive Rehabilitation Technology (SMART) Network, University of Alberta, Edmonton, Alberta, Canada. {J.Khodaeimehr, M.Sharifi, Mahdi.Tavakoli}@ualberta.ca

[2]Javad K. Mehr, Mojtaba Sharifi and Vivian K. Mushahwar are with the Department of Medicine, and Sensory Motor Adaptive Rehabilitation Technology (SMART) Network, University of Alberta, Edmonton, Alberta, Canada. Vivian.Mushahwar@ualberta.ca

Digital Object Identifier (DOI): see top of this page.

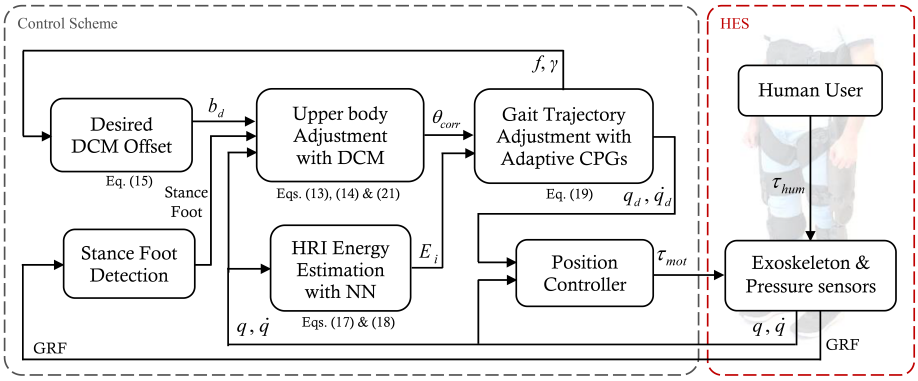

Fig. 1: Structure of the proposed intelligent control strategy with combination of DCM and CPG schemes for upper body adjustment and trajectory shaping

The central pattern generators (CPGs) has been also employed as connected modules for locomotion planning of bio-inspired robots due to its ability to produce synchronized rhythmic motions for multiple joints [12], [13]. Fang et al. [14] designed a CPG structure optimized by a genetic algorithm (GA) to generate the reference hip and knee trajectories for a multi-DOF exoskeleton. A similar GA-based scheme [15] was employed to facilitate steady-state locomotion for a lower-limb exoskeleton having specific CPG units for the knee stiffness regulation. Matsuoka-style CPGs [16] were proposed as another offline trajectory shaping integrated with fuzzy regulators for the exoskeleton's impedance variation. Zhang et al. [17] benefited from CPGs to provide fixed rhythmic trajectories for both the functional electrical stimulation and the torque controller of a knee rehabilitation system. However, having coupling between human and exoskeleton, it is essential to consider pHRI signals for the CPG-based trajectory shaping, which has not been investigated in previously developed schemes.

To enhance human authority and safety, intelligent control schemes have been developed to adapt the exoskeleton response to the human's physical behavior by monitoring the interaction torque between the human and the exoskeleton [18]. Accordingly, research studies have been dedicated to investigating intelligent strategies for the estimation of HRI force/torque (rather than direct measurement of them) using musculoskeletal models and artificial intelligence (AI) techniques. Linear proportional model [19] and Hill-type neuromusculoskeletal model [20], [21] are two of the commonly used approaches for the HRI estimation applications. However, due to the complexity of these models and the requirement of online parameter calibration, most of the recent studies have focused on the employment of AI-based techniques. Given the model-free learning feature of neural networks (NNs), they have been used to estimate HRI torque, shape the motion trajectory and determine the gait phase for lower-limb exoskeletons [22]. Radial basis function neural networks (RBFNNs) were also utilized to estimate the passive and active portions of the HRI torque in [23].

In the present study, an intelligent control strategy was developed and tested for lower-limb exoskeletons by introducing a new integration of DCM and CPG schemes to facilitate both postural stability and adaptive locomotion planning. The DCM analysis, which was previously developed for bipedal locomotion of humanoid robots, was extended and generalized for the human-exoskeleton system (HES) for the first time. To this end, the LIPF model was replaced with a new 4-DOF body (4DB) model to address the following issues: (a) In the LIPF model, the CoM of the whole system is considered to be at the middle of the line that connects the right and left hips. However, for the humans, the CoM is mostly higher than this level and can be different for users based on their body characteristics. Taking 4DB model into account, the CoM of combination HES can be at any point higher or lower than this level. (b) Due to the attachment of exoskeleton to the human body, the mechanical properties (e.g., moment of inertia and mass) for different segments of the HES can be significantly different for various wearers. Using the proposed 4DB model, these dynamic parameters can be personalized for each user to make the locomotion control strategy case-specific.

Using the proposed DCM analysis, a hip joint correction was generated in real-time to amend the trunk position and consequently adjust the DCM on its desired value at the end of each step. New adaptable CPGs were defined to shape joint trajectories in response to the human interaction torques by regulating the amplitude and frequency of walking. In addition, the CPG dynamics was designed to guarantee that gait frequency is less than the maximum stable frequency of walking and the output trajectories are within the feasible movement ranges of the exoskeleton joints. Accordingly, the set of commands generated by the DCM and CPG schemes were combined to autonomously facilitate locomotion trajectories that are compatible with the user's intention (active interaction) and also ensure the viability of walking through postural stability. The NARX neural network was employed to learn the passive dynamics of the HES in offline training sessions. Various position and velocity trajectories (inputs), and associated joint torques (outputs) of the multi-DOF exoskeleton were fed to this NN for training. The network was then used to estimate the active portion of the human interaction torque online and obtain HRI energy for the CPG-based trajectory shaping. The rest of the paper is organized as follows. The DCM and CPG formulations for upper-body and gait adjustments are described in Section II. The experimental

results of the proposed strategy having an able-bodied wearer are demonstrated and discussed in Section III, and concluding remarks are mentioned in Section IV.

II. Methodology

In this section, the mathematical formulations and different components of the proposed intelligent control strategy with their interconnections are explained. Using this strategy, the exoskeleton's wearer has the authority to adjust and personalize the gait parameters by applying torques and CPGs that translate this HRI into complaint locomotion trajectories. In order to guarantee the viability of walking, the exoskeleton modifies the upper body position using a hip correction approach based on a new DCM analysis. The structure of this control strategy with the combination of DCM and CPG schemes is shown in Fig. 1.

A. DCM Analysis with 4DB Model

The linear inverted pendulum flywheel model has been widely used to simulate and analyze bipedal walking for humanoid robots. In this model, the center of mass is considered to be exactly in the middle of the imaginary line that connects the right and left hip joints. Also, the mass-less inverted pendulum and flywheel represent the legs and upper body, respectively, which are simplistic assumptions. To study a collaborative human-exoskeleton walking, due to the human body characteristics, the center of mass can be at any point (not necessarily the hip joint). In order to address this issue, a new 4-DOF body (4DB) model was developed to represent the bipedal locomotion of the HES. As demonstrated in Fig. 2, the first link represents the stance leg, which is pivoted on the ground at the foot's center of pressure (CoP). The second segment in this model is the upper body, and the third and fourth links are devoted to the thigh and shank of the swing leg. The center of mass (CoM) of the HES is person-specific, which can be obtained based on the mechanical specifications of the user and exoskeleton. Using the Euler-Lagrange equation, the motion dynamics of the 4DB model was derived as

$$\overbrace{\begin{bmatrix} M_{11} & M_{12} & M_{13} & M_{14} \\ M_{12} & M_{22} & M_{23} & M_{24} \\ M_{13} & M_{23} & M_{33} & M_{34} \\ M_{14} & M_{24} & M_{34} & M_{44} \end{bmatrix}}^{M} \overbrace{\begin{bmatrix} \ddot{q}_1 \\ \ddot{q}_2 \\ \ddot{q}_3 \\ \ddot{q}_4 \end{bmatrix}}^{\ddot{q}} + \overbrace{\begin{bmatrix} G_{11} & G_{12} & G_{13} & G_{14} \\ 0 & G_{22} & G_{23} & G_{24} \\ 0 & 0 & G_{33} & G_{34} \\ 0 & 0 & 0 & G_{44} \end{bmatrix}}^{G} \overbrace{\begin{bmatrix} \cos(q_1) \\ \cos(q_1+q_2) \\ \cos(q_1+q_2+q_3) \\ \cos(q_1+q_2+q_3+q_4) \end{bmatrix}}^{p} = \overbrace{\begin{bmatrix} 0 \\ \tau_c \\ 0 \\ 0 \end{bmatrix}}^{\tau} \tag{1}$$

where the elements of the inertia (M) and gravity (G) matrices are defined in the Appendix. Note that in the derivation of the 4DB model, the segments were considered to be close to their vertical positions ($q_1 \simeq \frac{\pi}{2}$, $q_2, q_3, q_4 \simeq 0$) in the upright configuration of the body. Similar assumptions were considered in the previous models, e.g., LIP and LIPF [7],

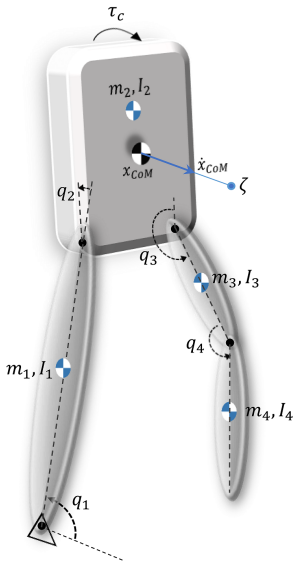

Fig. 2: Schematic of the proposed 4-DOF body (4DB) model for DCM analysis

[6]. Given the 4DB model, the position and acceleration of the Center of Mass (CoM) are

$$x_{CoM} = \overbrace{\begin{bmatrix} \varphi_1 & \varphi_2 & \varphi_3 & \varphi_4 \end{bmatrix}}^{\varphi} [p] \tag{2}$$

$$\ddot{x}_{CoM} = \overbrace{\begin{bmatrix} -\varphi_1-\varphi_2-\varphi_3-\varphi_4 \\ -\varphi_1-\varphi_2-\varphi_3 \\ -\varphi_1-\varphi_2 \\ -\varphi_1 \end{bmatrix}^T}^{\psi} \begin{bmatrix} \ddot{q}_1 \\ \ddot{q}_2 \\ \ddot{q}_3 \\ \ddot{q}_4 \end{bmatrix} \tag{3}$$

in which φ_i for $i = 1-4$ are defined as

$$\varphi_1 = \frac{m_1 l_{c1} + m_2 l_1 + m_3 l_1 + m_4 l_1}{\sum_{i=1}^{4} m_i} \quad \varphi_2 = \frac{m_2 l_{c2}}{\sum_{i=1}^{4} m_i}$$
$$\varphi_3 = \frac{m_3 l_{c3} + m_4 l_3}{\sum_{i=1}^{4} m_i} \quad \varphi_4 = \frac{m_4 l_{c4}}{\sum_{i=1}^{4} m_i} \tag{4}$$

Given (1), the joint acceleration vector can be summarized as

$$\ddot{q} = M^{-1}[\tau - Gp] \tag{5}$$

Note that the inertia matrix M is positive definite and always invertible. Therefore, substituting (5) into (3), the acceleration of CoM is obtained as

$$\ddot{x}_{CoM} = \psi M^{-1}\tau - \psi M^{-1} G p \tag{6}$$

Having (2), the acceleration of CoM can be rewritten as a function of the CoM position (x_{CoM}) and the torque applied to the trunk (τ) as

$$\ddot{x}_{CoM} = \alpha x_{CoM} + \beta\tau \tag{7}$$

where α and β are

$$\alpha = -\psi H x_{CoM} \qquad \beta = \psi M^{-1} \tag{8}$$

and $H = M^{-1} G \varphi^{\dagger}$, in which $\varphi^{\dagger}$ is the right pseudo-inverse of φ, defined as $\varphi^{\dagger} = \varphi^T(\varphi\varphi^T)^{-1}$.

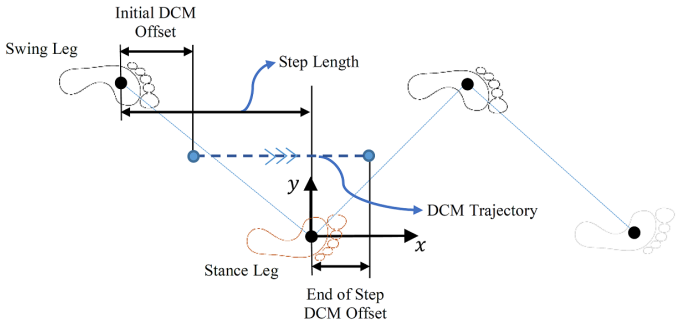

Fig. 3: Demonstration of footprints and DCM trajectory and offset during locomotion

Similar to the definition proposed in Jeong et al. [6], the extended DCM for the new 4DB model is defined as (see Appendix for detailed description)

$$\zeta = x + \frac{\dot{x}}{\sqrt{\alpha}} \tag{9}$$

Substituting the CoM acceleration in the 4DB model (7) into the time derivative of (9), the extended DCM dynamics is obtained as

$$\dot{\zeta} = \sqrt{\alpha}(\zeta + \frac{\beta}{\alpha}\tau) \tag{10}$$

In order to facilitate stable locomotion, the DCM value (ζ) at the end of each gait cycle needs to be controlled [24]. To this end, an optimization problem was defined to minimize the error between the actual and desired values of the DCM at the end of each step by adjusting the correction torque applied to the upper body.

$$\min_{\tau_c} \quad w_1||\tau_c||_2^2 + w_2||\zeta_T - \zeta_{T_d}||_2^2 \tag{11}$$

where ζ_T and ζ_{T_d} are the actual and desired end-of-step values of the DCM, respectively, and w_1 and w_2 are the optimization gains. Due to the attachment of the relative reference frame to the stance foot (shown Fig. 3), the desired DCM value at the end of the step (ζ_{T_d}) is equal to the desired DCM offset at that moment (b_d), which is defined in the next section.

B. DCM Offset for Viability of Walking

The DCM offset was defined as the difference between the landing location of the foot at the end of its swing phase and the point that DCM arrives at the end of that step. This offset is known as the key factor to address the most important characteristic of the bipedal locomotion, which is postural stability ensuring the viability of walking [8]. For instance, the higher gait velocities require larger DCM offset values and vice versa [6]. Figure 3 depicts the schematic of footprints and DCM offset in one stride.

The desired DCM offset for the 4DB model was determined based on the amplitude and frequency characteristics of the walking as described by Jeong et al. [6], and Khadiv et al. [25]

$$b_d = \frac{L}{e^{\sqrt{\alpha}T} - 1} \tag{12}$$

where L is the stride length and T is the step time. By reaching the desired offset value at the end of the step, in the absence of any disturbance, the CoM will travel the desired distance during the next step [8]. Using the CPG dynamics in the proposed strategy, the user can modify the amplitude and frequency of locomotion based on his/her desired gait pattern, by applying HRI torque. Therefore, the desired DCM offset will be affected by any change in the amplitude and frequency of walking. Accordingly, the physical HRI can alter the desired DCM value/offset at the end of each step.

Considering the kinematic and dynamic constraints of the human-exoskeleton system, the maximum possible DCM offset is calculated as

$$b_{max} = \frac{L_{max}}{e^{\sqrt{\alpha}T_{min}} - 1} \tag{13}$$

where L_{max} is the maximum feasible stride length and T_{min} is the minimum step time.

C. CPG Dynamics for Synchronized and Feasible Locomotion

Adaptive CPG dynamics was used for shaping stable gait parameters based on the HRI. In order to prevent the loss of postural stability during locomotion, threshold terms were added to the CPG dynamics to confine the amplitude and frequency of walking to the kinematic limits of the human-exoskeleton system. Therefore, the user has the authority to adjust the gait parameters over the stable limit by applying the interaction torque. In order to determine the HRI torque, an autoregressive network with exogenous inputs (NARX) was used to learn the passive dynamics of human limbs and exoskeleton. To collect motion and motor actuation data, a neurologically intact user was asked to walk with an exoskeleton over the ground for several trials. The data were classified for the stance phases of the right and left legs based on heel strike moments from pressure sensors embedded in insoles. Also, the user was asked to not apply any active interaction torque, so that the whole system was actuated using the motor torque applied to the joints. The position, velocity and torque values of the joints were collected for different frequency and amplitude values to be used for training the NARX. For the training process, the position and velocity of the joints were considered as the inputs $u(t)$, and the motor toques of the joints as the output $y(t)$. The trained NARX had the capability of estimating the passive dynamics of the human limbs and exoskeleton (τ_{pass}) during the online experimental process. Therefore, the interaction torque was determined as the difference between the current joint torque of the joint (τ_i) and the passive joint torque that was estimated by the NARX (τ_{pass}) as [26]

$$\tau_{HRI_i} = \tau_i - \tau_{pass} \tag{14}$$

Given the HRI torque, the HRI energy for each joint i was determined by taking the time integral of the multiplication of HRI torque and velocity as

$$E_i(t) = \int_0^t \tau_{HRI_i}(t)\ \dot{q}_i(t)\ dt \tag{15}$$

in which $\dot{q}_i(t)$ is the velocity and $\tau_{HRI_i}(t)$ is the estimated human torque of the joint $i = 1, ..., n$. When the interaction

torque had the same sign as velocity, the applied torque accelerated and when they had opposite signs, this torque caused deceleration of walking. The adaptive CPG dynamics for the joint trajectory generation, considering maximum gait frequency and amplitude, was defined as

$$\begin{aligned}\dot{\theta}_i(t) &= f(t) + \sum_{j=1}^{m_i} v_{ij}\, sin(\theta_i(t) - \theta_j(t) - \phi_{ij}) \\ \ddot{f}(t) &= \mu_f(\frac{\mu_f}{4}(F + \sum_{k=1}^{n} \eta_k E_k - f(t)) - \dot{f}(t)) \\ &\quad - k_f \frac{DZ^+(f(t) - f_{th})}{(f_{max} - f(t))^3} \\ \ddot{\gamma}(t) &= \mu_\gamma(\frac{\mu_\gamma}{4}(A + \sum_{k=1}^{n} \lambda_k E_k - \gamma(t)) - \dot{\gamma}(t)) \\ &\quad - k_\gamma(t) \frac{DZ^+(\gamma(t) - \gamma_{th})}{(\gamma_{max} - \gamma(t))^3}\end{aligned} \tag{16}$$

where m_i is the number of adjacent joints to the joint i, and n is the number of all joints. f_{max} and γ_{max} are the maximum frequency and amplitude values considered based on the motion constraints of the exoskeleton and walking safety concerns. If the frequency and amplitude exceed their threshold values f_{th} and γ_{th}, the dead-zone function DZ^+ is triggered to control them below their maximum values. Note that $DZ^+(x) = x$ for positive values of x and $DZ^+(x) = 0$ for any non-positive x. The η_k and λ_k are constant gains for the effect of HRI energy on the locomotion frequency and amplitude, respectively. v_{ij}, μ_f and μ_γ are other constant parameters of the dynamics. Using (16), the knee joint i's desired trajectory was formulated as

$$q_{d_i}(t) = \gamma(t)(a_{i_0} + \sum_{l=1}^{N_i}(a_{i_l} \cos(l\theta_i(t)) + b_{i_l} \sin(l\theta_i(t))) \tag{17}$$

where a_{i_l} and b_{i_l} are the coefficients of the Fourier series (with N_i terms) to initially coordinate the desired knee trajectory of the joint i with a typical one, as presented in Fig. 1.

The correction trajectory for the hip joints is affected by the obtained torque from the DCM adjustment strategy (see Eq. (11)).

$$\tau_c = J\ddot{\theta}_{corr} \tag{18}$$

where J is the moment of inertia for the upper-body of HES. By integrating the DCM torque in (18) over time, the trajectory correction for the hip joints (θ_{corr}) was determined. This time-varying correction adjusts the upper body position to reach the desired DCM value at the end of each step. Therefore, the desired trajectories of the stance and swing legs' hip joints were defined in terms of variables in (16) and (18) as

$$\begin{aligned}q_{d_{h_{ST}}}(t) &= \gamma(t)(a_{i_0} + \sum_{l=1}^{N_i}(a_{i_l} \cos(l\theta_i(t)) + b_{i_l} \sin(l\theta_i(t))) \\ &\quad + \theta_{corr} \\ q_{d_{h_{SW}}}(t) &= \gamma(t)(a_{i_0} + \sum_{l=1}^{N_i}(a_{i_l} \cos(l\theta_i(t)) + b_{i_l} \sin(l\theta_i(t))) \\ &\quad - \theta_{corr}\end{aligned} \tag{19}$$

where $q_{d_{h_{ST}}}$ and $q_{d_{h_{SW}}}$ are the desired trajectories of stance and swing legs' hip joints, respectively.

Given all of the desired joint trajectories, which are generated in real-time from the combination of DCM and CPG schemes, a position tracking controller can be employed to follow this comfortable and safe locomotion. Note that because of the CPG dynamics, the wearer has enough authority to adjust the gait parameters, but the intelligent controller of the exoskeleton limits the amplitude and frequency to ensure the viability of walking. Figure 1 demonstrates the structure of the proposed autonomous trajectory shaping and postural stability control.

III. Results & Discussion

In order to evaluate the effectiveness of the proposed autonomous trajectory shaping strategy, experimental studies were conducted using the Indego lower-limb exoskeleton (Parker Hannifin Corporation) [27] and an able-bodied human subject (height: 173 cm; weight: 67 kg) shown in Fig. 4. Note that the body characteristics of the exoskeleton wearer in (1) were estimated based on the provided formulations in Winter [28] according to the height and weight of the subject. The subject is asked to put a safety harness on, which is connected to an overhead lift to prevent injury in the case of falling. Real-time Desktop Simulink was utilized as the control software to implement the proposed intelligent control strategy (it received the sensory data, processed them and commanded the motor torques) on the exoskeleton with a sampling frequency of 100 Hz. For following the generated online trajectory, the built-in proportional-derivative (PD) position controller of the Indego was employed with appropriately adjusted gains. A pair of insole pressure sensors were embedded inside the shoes for detecting heel strike and stance leg to switch the pivot point of the 4DB model (Fig. 2) between the right and left legs. As soon as the switching of the stance phase occurred from one leg to the other, all DCM calculations switch correspondingly such that the pivot point, shifted to the new stance foot.

The experimental results are presented in two parts. In the first part, trunk position adjustment using the proposed DCM analysis was evaluated for postural stability. In the second section, the effect of human interaction torque on the CPG-based shaping of the gait characteristics (frequency and amplitude) and providing safe locomotion trajectories was investigated. The parameters of the DCM dynamics (10) were determined as $\alpha = 4.95$ and $\beta = 0.76$ based on the mechanical properties identified for the HES. The optimization gains were also specified as $w_1 = 10^{-7}$ and $w_2 = 1$ using a trial-and-error method to have an appropriate trade-off between the obtained torque (τ_c) for the trunk and the DCM error ($\zeta_T - \zeta_{T_d}$) at the end of a step.

A. Trunk Adjustment Using DCM Analysis

The desired DCM offset value at the end of each step was a function of the step length and total frequency of walking based on Eq. (12). Due to the variation of landing positions, the optimization approach (Sec. II-A) was utilized to obtain the upper-body torque (τ_c) and determine the hip trajectory

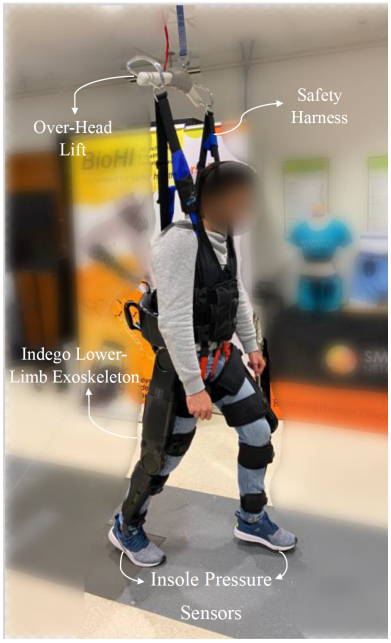

Fig. 4: Experimental set-up: Indego lower-limb exoskeleton in a user study (having a safety harness) during over-ground walking

correction (Eq. 18) in order to minimize the DCM error at the end of each step. The correction value of the upper body position (θ_{corr}) was added to the reference CPG trajectory for the hip joint of the stance leg. Note that, the negative value of the θ_{corr} was added to the reference CPG trajectory of the hip joint of the swing leg, in order to not affect the swing trajectory of the walking.

The primary amplitudes of the hip and knee motions were considered 59 and 70 degrees, and the locomotion frequency was set to 2.6 rad/s based on typical gait cycles. Figure 5 represents trajectories of the right and left hips with and without applying the DCM correction for them. This motion correction at the beginning of the stance phase of each leg decreased the desired hip angle of that leg. As seen in Fig. 5, the desired trajectory of the swing leg's hip was also increased in the opposite direction to preserve the landing position of the next step (as described in Sec. II-C). The landing moments of the left and right feet are pointed out in Fig. 5, where the acceleration of hip corrections was changed. This behavior is also illustrated in Fig. 6, where the modifications can be seen in the relative motion of the hips. From the beginning of the stance phase, the synchronization of the right and left hip joints became distorted as highlighted in Fig. 6.

In order to elaborate more on the trunk position correction obtained from the DCM analysis, Fig. 7 depicts the DCM values for the stance phases of the right and left legs. Note that in the calculation of DCM magnitude, the stance foot's CoP was considered as the Cartesian coordinates' origin (shown in Fig. 3). As seen in Fig. 7, for the first four steps of walking ($t = 0 - 5.17\ s$), the DCM has a disorganized translation from the initial value to the end-of-step one due to the wearer's interaction with the exoskeleton. In order to minimize the DCM end-of-step error, the highest position

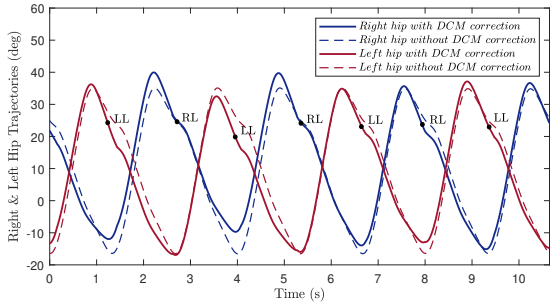

Fig. 5: Right and left hip trajectories in the presence and absence of DCM corrections

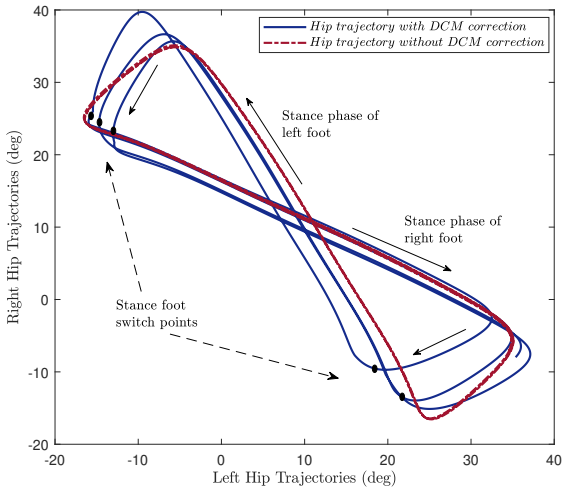

Fig. 6: Relative motion of the right and left hips with and without considering DCM corrections

correction for upper body was suggested during this period in comparison to the latest four steps as observed in Fig. 5. Similarly, in all of the other steps of walking, the upper body's position correction adjusted the hip joints' trajectories generated by CPGs to reach the desired DCM value at the end of each step. In order to evaluate how the end-of-step DCM error was affected by the upper body adjustment, the result of DCM values in the absence of applying the proposed DCM correction was investigated in another experiment. As demonstrated in Fig. 8, the average end-of-step error without upper body adjustment was 0.05 m, which was considerable and caused unstable walking that would raise the risk of falling down without employing a safety harness. However, using the proposed DCM correction strategy, this error was reduced to 0.002 m and the DCM trajectory experienced more organized variations (Fig. 5).

The desired trajectories for the hip and knee joints, obtained from the combined CPG and DCM schemes, were commanded to a PD position controller to be tracked by the exoskeleton. The performance of this controller in following the desired values of the right hip and knee (with the maximum errors of 0.6 $degree$ and 1.1 $degrees$, respectively) are shown in Fig. 9.

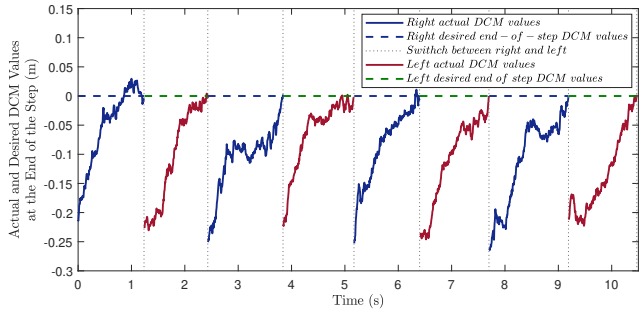

Fig. 7: Actual and desired end-of-step values of DCM for right and left feet in the presence of DCM correction

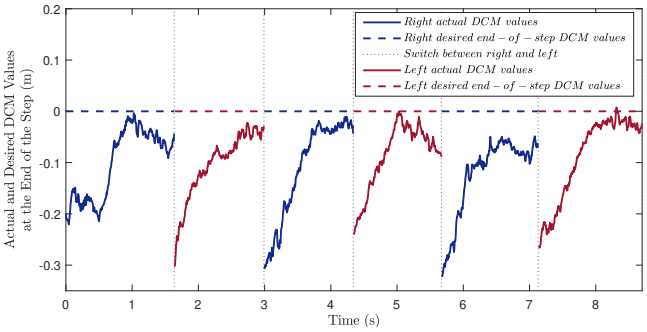

Fig. 8: End-of-step values of DCM in the absence of DCM correction

B. Locomotion Shaping with Maximum Walking Frequency

The performance of the proposed CPGs in online shaping of gait parameters was investigated while preserving the postural stability. During this experiment, the wearer applied accelerating torques on different joints in order to speed up his walking. Although he was able to increase the amplitude and frequency of locomotion, the threshold and maximum values of these variables were set to be $\gamma_{th} = 1.1$, $\gamma_{max} = 1.2$ and $f_{th} = 1.04\pi\ rad/s$, $f_{max} = 1.08\pi\ rad/s$ in (16) based on practical limitations of the exoskeleton movement and the safety of the human user. As seen in Fig. 10(a), the total gait amplitude γ increased and reached its threshold value at $t = 0.85\ s$. After this time, the threshold regulation term in (16) was activated to detract the increment rate of the amplitude and saturate it around 1.19 at $t = 14.5\ s$. Similar behavior can be seen in Fig. 10(b) for the total frequency of walking according to (16), where its threshold regulation term was triggered at $t = 2.15\ s$ and then the frequency is saturated below $f_1(t) = 3.39\ rad/s$ until $18.5\ s$. Also, in order to further evaluate the effectiveness of CPG in facilitating the user's intention, the wearer could change the frequency of walking to a desired value less than the threshold in another experiment. As seen in Fig. 10(b), the total frequency of walking reached the desired value of $f_2(t) = 2.4\ rad/s$ at $t = 7.5\ s$ and the user retained this walking frequency for the rest of his locomotion.

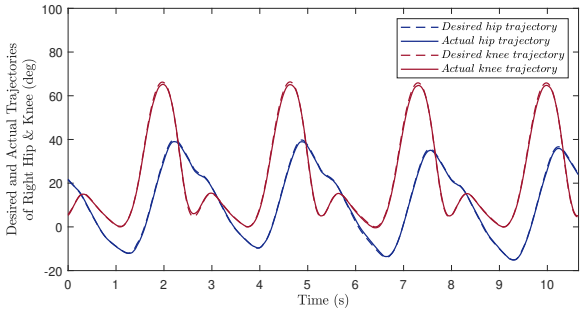

Fig. 9: Performance of the position controller in tracking the desired right hip and knee trajectories

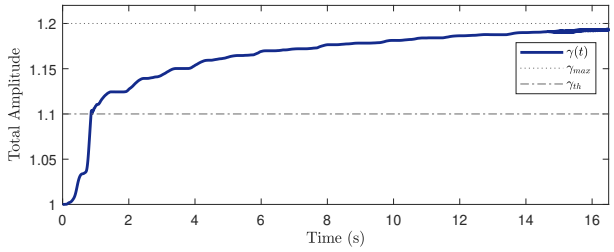

(a)

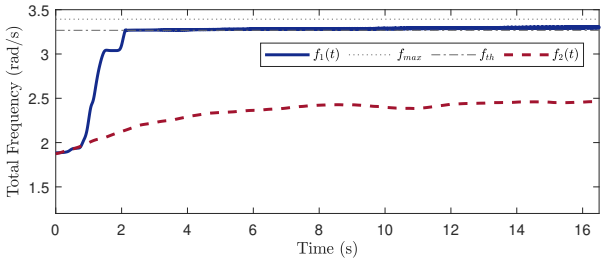

(b)

Fig. 10: Control of (a) the amplitude and (b) the frequency of locomotion between their threshold and maximum values using CPG dynamics

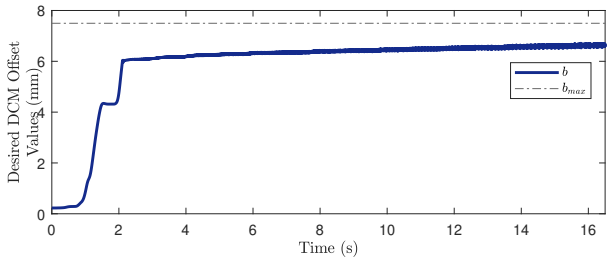

Fig. 11: Variation of DCM offset below its maximum value

As discussed in Sec. II-B, the DCM offset is a function of the walking frequency and the step length. Given the maximum feasible amplitude and frequency of walking as $\gamma_{max} = 1.2$ and $f_{max} = 1.08\pi\ rad/s$, the maximum DCM offset was obtained as $b_{max} = 7.5\ mm$. As is observed in Fig. 11, after $t = 2.17\ s$ both amplitude and frequency threshold terms were activated in (16), the variation rate of b_d decreased drastically and finally plateaued at $t = 18.5\ s$ around $6.6\ mm$ which is less than the maximum offset value ($b_{max} = 7.5\ mm$).

IV. Conclusions

In the present study, a novel intelligent control strategy was developed for the human exoskeleton system, which can revise the locomotion trajectories in real-time for preserving postural stability. In the proposed shared autonomy between

the human and robot, the user has the authority of adjusting the amplitude and frequency of walking, while the exoskeleton has enough autonomy to correct the trunk position to guarantee the viability of walking and limit the gait amplitude and frequency within their feasible ranges. For these purposes, the DCM analysis was extended by presenting a new 4-DOF body (4DB) model to be compatible with the human-exoskeleton system's dynamics. Taking the advantage of this 4DB model, the locomotion control was personalized by considering the dynamic parameters of the body segments (moment of inertia, mass and CoM) for each user.

The HRI torque was employed in the adaptable CPG structure to update the locomotion based on the user's intention. Also, the desired DCM value at the end of each step was calculated based on the user's demanded amplitude and frequency, which is facilitated by adjusting the upper body position using a hip correction strategy for the exoskeleton. To this end, an optimization problem was defined to minimize the DCM end-of-step error by determining the required upper body motion correction that should be added to the desired gait trajectories. This revised trajectory generated by combination of DCM and CPG schemes was tracked by the exoskeleton's motor controller. The proposed strategy was tested experimentally on the Indego lower-limb exoskeleton, and the obtained results proved its effectiveness in providing postural stability and the adaptation of gait motion. Accordingly, this control method enhanced the user's safety and comfort in walking (as one of the most essential activities) using an assistive exoskeleton by offering a trade-off between the robot autonomy and human authority. The upper-body position adjustment was designed to provide postural stability with slight changes in the gait parameters (amplitude and frequency) in response to the active HRI torque. However, for the case of large disturbances, e.g., having a collision with the environment, an extended control approach with the ankle joint's actuation will be required. This strategy can be investigated in future studies using fully actuated exoskeletons.

APPENDIX

The elements of the inerta matrix and gravity vector, and the DCM formulation are provided in https://github.com/tbs-ualberta/Paper_DCM_Lower-limb_Exo.git.

REFERENCES

[1] A. Martínez et al., "A velocity-field-based controller for assisting leg movement during walking with a bilateral hip and knee lower limb exoskeleton," *IEEE Trans. Robot.*, vol. 35, no. 2, pp. 307–316, 2019.

[2] L. Zhou et al., "A novel precision measuring parallel mechanism for the closed-loop control of a biologically inspired lower limb exoskeleton," *IEEE/ASME Trans. Mechatron.*, vol. 23, no. 6, pp. 2693–2703, 2018.

[3] V. Azimi et al., "Robust ground reaction force estimation and control of lower-limb prostheses: Theory and simulation," *IEEE Trans. Syst. Man Cybern. Syst.*, vol. 50, no. 8, pp. 3024–3035, 2020.

[4] M. Shafiee-Ashtiani et al., "Robust bipedal locomotion control based on model predictive control and divergent component of motion," in *ICRA*, 2017, pp. 3505–3510.

[5] T. Kamioka et al., "Simultaneous optimization of zmp and footsteps based on the analytical solution of divergent component of motion," in *ICRA*, 2018, pp. 1763–1770.

[6] H. Jeong et al., "A robust walking controller based on online optimization of ankle, hip, and stepping strategies," *IEEE Trans. Robot.*, vol. 35, no. 6, pp. 1367–1386, 2019.

[7] T. Takenaka et al., "Real time motion generation and control for biped robot -1st report: Walking gait pattern generation-," in *IROS*, 2009, pp. 1084–1091.

[8] M. Khadiv et al., "A robust walking controller based on online step location and duration optimization for bipedal locomotion," *CoRR*, vol. abs/1704.01271, 2017. [Online]. Available: http://arxiv.org/abs/1704.01271

[9] H. Jeong et al., "A robust walking controller optimizing step position and step time that exploit advantages of footed robot," *Robot. Auton. Syst.*, vol. 113, pp. 10–22, 2019.

[10] J. Englsberger et al., "Three-dimensional bipedal walking control based on divergent component of motion," *IEEE Trans. Robot.*, vol. 31, no. 2, pp. 355–368, 2015.

[11] Q. Li et al., "Contact force/torque control based on viscoelastic model for stable bipedal walking on indefinite uneven terrain," *IEEE Trans. Autom. Sci. Eng.*, vol. 16, no. 4, pp. 1627–1639, 2019.

[12] A. Ijspeert et al., "From swimming to walking with a salamander robot driven by a spinal cord model," *Science*, vol. 315, no. 5817, pp. 1416–1420, 2007.

[13] A. Sproewitz et al., "Learning to move in modular robots using central pattern generators and online optimization," *Int. J. Rob. Res.*, vol. 27, no. 3-4, pp. 423–443, 2008.

[14] J. Fang et al., "A robotic exoskeleton for lower limb rehabilitation controlled by central pattern generator," in *ROBIO*, 2014, pp. 814–818.

[15] S. Schrade et al., "Bio-inspired control of joint torque and knee stiffness in a robotic lower limb exoskeleton using a central pattern generator," in *ICORR*, 2017, pp. 1387–1394.

[16] R. Luo et al., "Adaptive cpg-based impedance control for assistive lower limb exoskeleton," in *ROBIO*, 2018, pp. 685–690.

[17] D. Zhang et al., "Cooperative control for a hybrid rehabilitation system combining functional electrical stimulation and robotic exoskeleton," *Front. neurosci.*, vol. 11, p. 725, 2017.

[18] M. Sharifi et al., "Impedance variation and learning strategies in human-robot interaction," *IEEE Trans. Cybern.*, pp. 1–14, 2021.

[19] T. Teramae et al., "Emg-based model predictive control for physical human-robot interaction: Application for assist-as-needed control," *IEEE RAL*, vol. 3, no. 1, pp. 210–217, 2017.

[20] D. Xu et al., "Development of a semg-based joint torque estimation strategy using hill-type muscle model and neural network," *J. Med. Biol. Eng.*, pp. 1–11, 2020.

[21] D. Ao et al., "Movement performance of human–robot cooperation control based on emg-driven hill-type and proportional models for an ankle power-assist exoskeleton robot," *IEEE Trans. on Neural Syst. Rehabilitation Eng.*, vol. 25, no. 8, pp. 1125–1134, 2016.

[22] X. Wu et al., "Individualized gait pattern generation for sharing lower limb exoskeleton robot," *IEEE Trans. Autom. Sci. Eng.*, vol. 15, no. 4, pp. 1459–1470, 2018.

[23] K. Gui et al., "A practical and adaptive method to achieve emg-based torque estimation for a robotic exoskeleton," *IEEE/ASME Trans. Mechatron.*, vol. 24, no. 2, pp. 483–494, 2019.

[24] T. Takenaka et al., "Real time motion generation and control for biped robot -1st report: Walking gait pattern generation-," in *IROS*, 2009, pp. 1084–1091.

[25] M. Khadiv et al, "Step timing adjustment: A step toward generating robust gaits," in *Humanoids*. IEEE, 2016, pp. 35–42.

[26] R. Gupta et al., "Continuous angular position estimation of human ankle during unconstrained locomotion," *Biomed. Signal Process. Control*, vol. 60, p. 101968, 2020.

[27] S. A. Murray et al., "Fes coupled with a powered exoskeleton for cooperative muscle contribution in persons with paraplegia," in *EMBC*, 2018, pp. 2788–2792.

[28] D. A. Winter, *Biomechanics and motor control of human movement*. John Wiley & Sons, 2009.